Quantitative Proton Spectroscopic Imaging of the Neurochemical Profile in Rat Brain with Microliter Resolution at Ultra-short Echo Times

Vladimír Mlynárik,[1][*] Ingrid Kohler,[1] Giulio Gambarota,[1] Anne Vaslin,[2] Peter G.H. Clarke,[2] and Rolf Gruetter[1]

Proton spectroscopy allows the simultaneous quantification of a high number of metabolite concentrations termed the neurochemical profile. The spin echo full intensity acquired localization (SPECIAL) scheme with an echo time of 2.7 ms was used at 9.4T for excitation of a slab parallel to a home-built quadrature surface coil in conjunction with phase encoding in the two remaining spatial dimensions to yield an effective spatial resolution of 1.7 μL. The absolute concentrations of at least 10 metabolites were calculated from the spectra of individual voxels using LCModel analysis. The calculated concentrations were used for constructing quantitative metabolic maps of the neurochemical profile in normal and pathological rat brain. Summation of individual spectra was used to assess the neurochemical profile of unique brain regions, such as corpus callosum, in rat for the first time. Following focal ischemia in rat pups, imaging the neurochemical profile indicated increased choline groups in the ischemic core and increased glutamine in the penumbra, which is proposed to reflect glutamate excitotoxicity. We conclude that it is feasible to achieve a sensitivity that is sufficient for quantitative mapping of the neurochemical profile at microliter spatial resolution. Magn Reson Med 59: 52–58, 2008. © 2007 Wiley-Liss, Inc.

Key words: proton magnetic resonance spectroscopic imaging; short echo time; metabolite concentrations; rat brain; cerebral ischemia

In the past decade we and others have established that proton MR localized spectroscopy with echo times on the order of 2 ms allows measuring metabolite concentrations in the brain (1–4). Approximately 18 metabolite concentrations that can be measured at 9.4T results in a neurochemical profile (2) consisting of putative markers implicated in myelination (phosphoethanolamine [PE], N-acetylaspartate [NAA], glycerophosphocholine, phosphocholine), osmolytes (taurine [Tau], myo-inositol [Ins], scyllo-inositol), antioxidants (glutathione and ascorbate [Asc]), energy metabolism (creatine [Cr] and phosphocreatine [PCr], glucose [Glc], lactate [Lac], and alanine [Ala]), and neurotransmitters and associated metabolites (γ-aminobutyrate [GABA], N-acetylaspartylglutamate [NAAG], glutamate [Glu], and glutamine [Gln]). Short echo time proton spectroscopy enables us to quantify compounds with spin systems including strongly and/or weakly J-coupled multiplets as well as singlet resonances without the need for correcting effects of T_2 relaxation times. Most studies to date have used single-voxel localized spectroscopy to obtain such neurochemical profiles only from one selected volume at a time.

On the other hand, spectroscopic imaging can be used to obtain this information simultaneously from many voxels, amounting to a regional mapping of the neurochemical profile. It is also likely to yield important insight in diseases with complex regional distribution of metabolites such as focal ischemia or multiple sclerosis. Most studies based on spectroscopic imaging techniques have used long echo times, thereby limiting the obtained concentrations to prominent singlets of NAA, total creatine (tCr), and choline-containing compounds (Cho), and in some cases to a few J-coupled resonances, such as Lac and glutamate + glutamine (Glx) (5,6) due to the additional signal loss incurred by J-modulation of strongly coupled spin systems.

A number of practical implementations of short-echo-time spectroscopic imaging in brain have been reported. In human studies short-echo-time measurements were used either for obtaining localized spectra and metabolite concentrations from specific regions of the brain (7–14) or for constructing qualitative metabolic maps of some metabolites (15). Only the article by McLean et al. (6) showed quantitative maps of NAA and Glx obtained with TE = 30 ms at 1.5T in a healthy human subject and in a multiple sclerosis patient.

A few reports describe short-TE spectroscopic imaging in animals, which was used for quantification of metabolites giving J-coupled multiplets. Juchem et al. (16) performed spectroscopic imaging experiments at 7T in the monkey brain with very high spatial resolution (4 μL) using the STEAM excitation scheme and TE = 10 ms. They quantified NAA, tCr, and Glx in gray and white matter of the visual cortex. Geppert et al. (3) demonstrated the feasibility of PRESS-based spectroscopic imaging with TE = 6 ms in rat brain. Liimatainen et al. (17) used ultra-short echo-time spectroscopic imaging experiment (TE = 2 ms) to map lipids in treated glioma in rats. The distribution of metabolites showing J-coupled multiplets was also mapped using a combination of 2D spectroscopic imaging with 2D correlation spectroscopy in a rat brain glioma

model (18,19). To our knowledge, *quantitative* maps of the neurochemical profile have not been reported to date.

In addition to the technical challenge of the intrinsically low sensitivity of NMR spectroscopy, spectroscopic imaging needs to contend with potential signal contamination from extraneous lipid and water signals. Sensitivity can be substantially improved by using a high magnetic field, optimized magnetic field homogeneity, and using ultra-short echo time. We have recently described such advances using the spin echo full intensity acquired localization (SPECIAL) (20) scheme single-voxel localization, affording about a 2-fold sensitivity gain over previous studies. We hypothesized that these advances in sensitivity would permit imaging the neurochemical profile at a spatial resolution comparable to that achieved with mapping cerebral metabolic rate of glucose in rodents using fluorodeoxyglucose positron emission microtomography. Therefore, the aim of the present study was to demonstrate the feasibility of quantitative mapping of the neurochemical profile consisting of at least 10 metabolites in rodent brain at 9.4T at about 2 ms echo time with a nominal spatial resolution of 1–2 μL.

MATERIALS AND METHODS

Animal Preparation

In vivo experiments were performed on male Sprague-Dawley rats, which were anesthetized with 1.5–2.5% isoflurane using a nose mask. All animal experiments were conducted according to federal and local ethical guidelines and the protocols were approved by the local regulatory body. Body temperature was maintained at 37.5 ± 1.0°C by circulating warm water around the animals. Two groups of animals were studied: The first consisted of three healthy adult rats with a mean weight of 280 g. In the second group, which involved three 13-day-old rats, focal ischemia was induced the day before by middle cerebral artery occlusion according to the protocol of Renolleau et al. (21). The main cortical branch of the left middle cerebral artery was electrocoagulated just below the bifurcation of the middle cerebral artery into frontal and parietal branches. The left common carotid artery was then occluded by means of a clip for 90 min. This increased the size of the lesion and reduced variability by causing a transient reduction of blood flow into the ischemic region via anastomoses from the anterior and posterior cerebral arteries. Thus, the ischemia involved both transient and permanent components. During surgery, rat pups were maintained at 37°C in the induction chamber under 2.5% isoflurane. The arterial clip was then removed and the restoration of carotid blood flow was verified under a dissecting microscope before the skin incision was closed. The final MR imaging was performed on the fourth day after the surgery. The rats were then perfused through the heart with 4% paraformaldehyde in phosphate-buffered saline. Cresyl violet-stained serial cryostat sections 50 μm thick were traced using a computer-microscope system equipped with the Neurolucida program (MicroBright-Field, Colchester, VT) and the volumes of the necrotic area were calculated.

MRI and Spectroscopic Imaging

Measurements were performed on a Varian INOVA spectrometer (Varian, Palo Alto, CA) interfaced to an actively shielded 9.4T magnet with a 31-cm horizontal bore (Magnex Scientific, Abingdon, UK) and with a 12-cm i.d. actively shielded gradient set to allow a maximum gradient of 400 mT/m in 120 μs. A home-built quadrature coil consisting of two geometrically decoupled 14-mm-diameter single loops was used as both transmitter and receiver. The static field homogeneity was adjusted using first- and second-order shims using an EPI version of FASTMAP (22).

Localizer images were obtained in the coronal and horizontal planes using a multislice turbo-spin-echo protocol (TR/TE = 2000/64 ms, echo train length = 8, field of view [FOV] = 24 mm × 24 mm, slice thickness = 0.7 mm, two averages, 128^2 image matrix). For spectroscopy, a rectangular volume with the typical dimensions of $10 \times 2 \times 10$ mm³ in the X, Y, and Z directions, respectively, was excited in the brain using the SPECIAL technique with TE = 2.7 ms (20). In short, 1D image-selected in vivo spectroscopy (ISIS) in the vertical (Y) direction was combined with a slice selective spin echo in the X and Z directions. The slice profile was optimized and the chemical shift displacement minimized for slice selection in the Y direction (parallel to the plane of the surface coil) by using a broadband (10 kHz) adiabatic full-passage pulse. Frequency offsets for slice-selective pulses were calculated relative to the center of the metabolite spectrum (2.3 ppm). Two free induction delays of 2048 complex points (spectral width of 5000 Hz, acquisition time 410 ms) with this adiabatic pulse on and off, respectively, were subtracted for each phase encoding step. The excited transverse magnetization was phase encoded in the X and Z dimensions using FOV = 24 mm × 24 mm and 32 × 32 phase encoding steps spanning a Cartesian sampling of *k*-space, resulting in a nominal in-plane resolution of 750 μm. For the metabolite maps, scans were performed using VAPOR water suppression interleaved with three modules of outer volume saturation as described elsewhere (1) using a TR of 2–2.5 sec. For absolute quantification, water reference maps were obtained with a TR of 1.5 sec by omitting the outer volume saturation and water suppression. The total measurement time including water referencing was 120 or 135 min.

Data Processing

An optimized Hanning *k*-space filter (23) was used in both spatial dimensions. This apodization increased the overall signal-to-noise ratio (SNR) and restricted Gibbs' ringing of the spatial response function to neighboring voxels at the expense of a slightly broadened central lobe of the spatial response function, which was conical in the 2D spatial domain with the full-width-at-half-maximum (the diameter of a circle) about 1.4 times greater than the linear voxel dimension (23). Thus, given the nominal voxel size of $l_X \times l_Z \times l_Y = 0.75 \times 0.75 \times 2.0 = 1.1$ mm³, the effective spatial resolution was $\pi \times (1.4 \times l_X/2)^2 \times l_Y = \pi \times (1.4 \times 0.75/2)^2 \times 2.0 = 1.7$ mm³. Concentrations of metabolites were calculated for each voxel in a rectangular region

consisting of 9 to 10 columns and 11 to 12 rows in the XZ plane using the water signal from the same voxel as reference. Horizontal dimensions of the excited volume were selected to be larger by 15–20% than the active volume of the surface RF coil, which reduced the chemical shift displacement error effects of the slice selective pulses in the X and Z directions.

The reference data basis for the LCModel (24) calculations comprised spectra of metabolite solutions as well as a spectrum of macromolecules and spectral lines of lipids at 0.9 and 1.3 ppm. Absolute metabolite concentrations were corrected for different repetition times in the water and metabolite scans and for the different T_1 relaxation times of water and metabolites assuming a T_1 of 1.9 sec for water and a mean value of 1.4 sec for the metabolites (25). For spectra from voxels lying in the region of the optimal sensitivity of the RF coil, the Cramer–Rao lower bounds were typically 2–4% for NAA, tCr, and Glu, 5–10% for Cho, Gln, Ins, Tau, and 10–20% for Lac, Glc, GABA, PE, and Asc.

RESULTS

The quality of FASTMAP shimming over the excited volume was evaluated from scans of healthy adult rat brain with an unsuppressed water signal. In the central part of the excited region the water linewidth was in the range of 10–15 Hz, and only a small number of voxels (typically 20–30%), especially in the outer part of the excited region, had a linewidth of more than 16 Hz.

The performance of the technique was tested on the brain of three healthy adult rats. Figure 1a shows horizontal and coronal views of the excited volume in the brain, which included various cerebral structures. Its rostral part (indicated by r in Fig. 1) contained mostly frontal cortex, combined with corpus callosum in small regions. The central part (m) included cortex and corpus callosum, which was dominant in some voxels. The major structure in the caudal part (c) of the excited region was the hippocampus, which contained in some voxels contributions from corpus callosum and/or cortex. Figure 1c shows an excerpt of 16 spectra from the central and caudal part of the excited region. By adding together six spectra from voxels containing almost pure cerebral structures, such as corpus callosum and hippocampus, the spectra of the respective tissues were obtained with an SNR increased by a factor about 1.8 compared to that from the individual voxels (Fig. 2). A visual inspection as well as LCModel calculations revealed that metabolite concentrations were lower in corpus callosum representing white matter than in hippocampus representing gray matter, with the differences being most marked for Ins (7.4 ± 0.2 mM and 5.4 ± 0.2 mM in hippocampus and corpus callosum, respectively, with the error limits being Cramer–Rao lower bounds calculated by LCModel), Tau (6.0 ± 0.2 mM and 4.8 ± 0.2 mM), tCr (9.6 ± 0.2 mM and 8.6 ± 0.2 mM), and for GABA (1.9 ± 0.1 mM and 1.4 ± 0.2 mM).

To illustrate the ability of the described spectroscopic imaging protocol to quantify changes of metabolite concentrations at very high spatial resolution, three rat pups subjected to middle cerebral artery occlusion were studied. Figures 3–5 show the results obtained on one of them
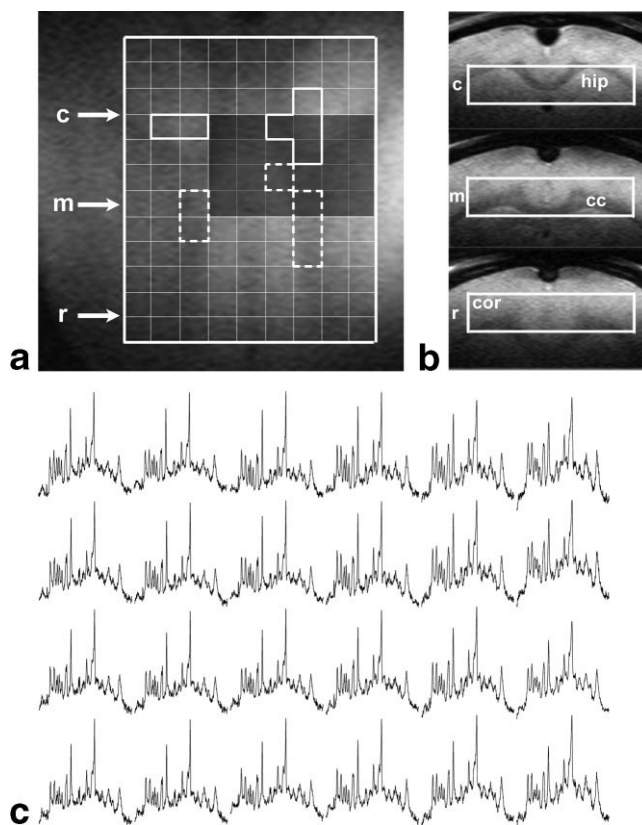

FIG. 1. Spectroscopic imaging scan of a healthy adult rat brain based on an excited volume of 10 × 2 × 10 mm³ and TE/TR = 2.7/2000 ms. (**a**) Horizontal and (**b**) coronal views (rostral [r], central [m], and caudal [c]) of the excited slab showing involved cerebral structures; cor, cortex; cc, corpus callosum; hip, hippocampus. (**c**) A series of water-suppressed proton spectra corresponding to the dark-shaded area in (**a**).

that is representative of all three studies conducted. Quantitative metabolic maps were measured 36 hr after the onset of ischemia in the brain region delineated in the T_2-weighted images in the first row of Fig. 3. Four days after the surgery, MRI delineated regression of the edema and an infarct region that extends into the lower right corner of the evaluated region (Fig. 4a,b). The volume of the infarct region calculated from histology was 36 mm³. The average concentrations of 10 metabolites measured in characteristic regions of all three rats were assessed in the infarct region, in the edema surrounding the necrotic core, in the normally appearing tissue adjacent to the edema (penumbra), and in the identical area of the contralateral hemisphere (Table 1). The quality of the achieved data is illustrated by two examples of the LCModel fit of spectra from voxels located in the edematous tissue and in penumbra (Fig. 5). Both Table 1 and metabolic maps in Fig. 3 showed more than a 50% reduction in absolute concentrations of almost all metabolites in the region corresponding to the hyperintense signal in T_2-weighted images, as illustrated for Cr, NAA, Glu, Gln, Cho, Tau, Ins, and Glc (second and third rows of Fig. 3). In contrast to the general concentration decreases, however, some metabolites showed a distinct increase in the affected hemisphere. The
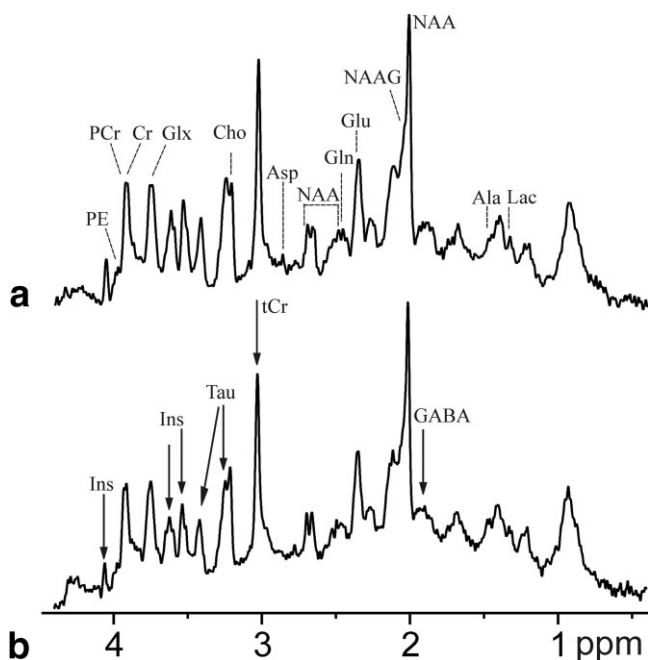
FIG. 2. Spectra of "pure" hippocampus (**a**) and corpus callosum (**b**) obtained by summing six voxels (delineated in Fig. 1 by solid lines for hippocampus and by dashed lines in corpus callosum) containing predominantly one type of the respective tissue and showing narrow water linewidth. Compared to spectra from individual voxels, the SNR increased from 13 to 25 in hippocampus (an increase of 90%) and from 12.8 to 22 in corpus callosum (+72%). Arrows in the spectrum of corpus callosum denote the most striking differences in spectral appearance, confirmed by LCModel analysis.
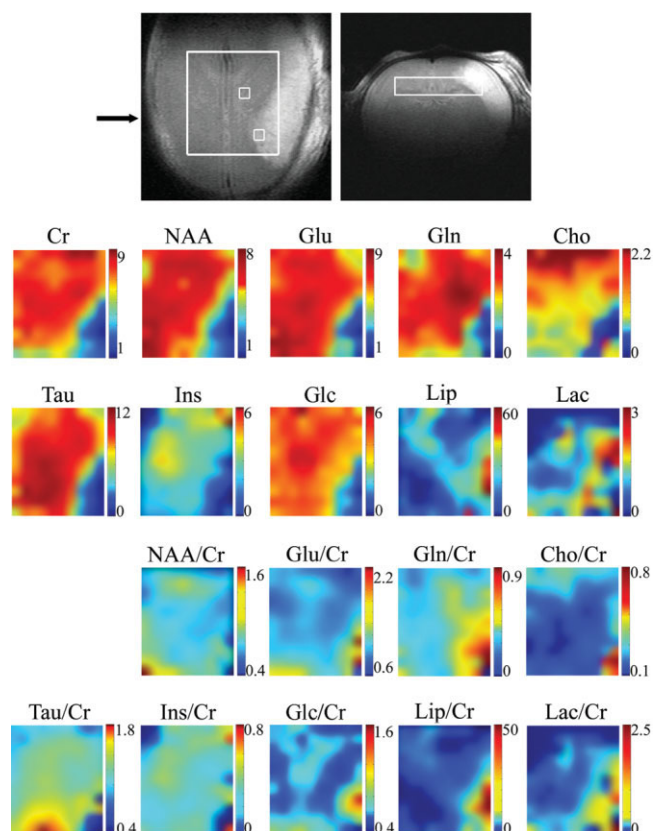

FIG. 3. High-resolution quantitative metabolite maps of a rat brain 36 hr after the onset of focal ischemia in the left cortex. The size of the excited volume was $9 \times 2 \times 8$ mm³, TE/TR = 2.7/2500 ms. The fast-spin-echo images (the first row) were measured immediately before the spectroscopic imaging scan. The rectangle defines the position of 10×11 voxels shown on metabolic maps, which is smaller than the excited volume to eliminate voxels prone to localization errors (such as limited excitation and chemical shift-displacement-error related effects). The position of the coronal image across the infarcted region is indicated by an arrow. Maps of absolute concentration of metabolites (in mmol/kg) as calculated by LCModel are shown in the second and third rows; maps of relative concentrations using the total Cr as a reference are given in the last two rows.

concentration of free lipids (Lip) was increased by 50–100% in the affected tissue. Interestingly, in what would later turn out to be the final necrotic region (Fig. 4c and hyperintensity in the lower right corner of the Cho map in Fig. 3), the Cho concentration was comparable to that in the penumbra and contralateral hemisphere (about 1 mmol/kg), whereas it was lower in the edematous tissue (about 0.4 mmol/kg). Gln, on the other hand, was increased by about 30% in penumbra relative to the contralateral hemisphere. A nonuniform increase of Lac was also observed in the tissue surrounding the affected area.

To minimize the effect of increased water content in the area surrounding the infarct region (26) on the metabolite quantification, metabolic maps of concentrations relative to that of total Cr were calculated (fourth and fifth rows of Fig. 3). While the NAA/Cr distribution was mostly uniform, the relative concentrations of other metabolites either increased or decreased in the affected area near the infarct. Outside this area they were uniform, showing no differences between the two hemispheres despite the fact that the 90-min occlusion of the common carotid artery greatly reduced blood flow throughout the entire left hemisphere. Glu/Cr increased by about 30% in the close vicinity of the region of infarct visible in Fig. 4. The relative concentrations of Tau and Ins decreased more than 60% in the region of the infarct. On the other hand, the increases in Glc/Cr, Lip/Cr, and particularly Gln/Cr were more widespread: Glc/Cr was higher in about 10% of the mapped

volume, Lip/Cr was elevated in about 20%, and Gln/Cr was higher in about 30–40% of the volume shown in the metabolic map. The relative concentration of Lac was elevated in about 20% of the mapped volume; however, the
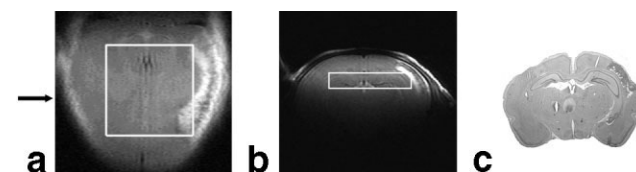

FIG. 4. Evolution of the hypoxic-ischemic lesion shown in fast-spin-echo images (**a,b**) of the rat brain from Fig. 3 measured 4 days after the onset of ischemia and (**c**) in the corresponding histological section. The position of the coronal image and the histological section is indicated by an arrow.
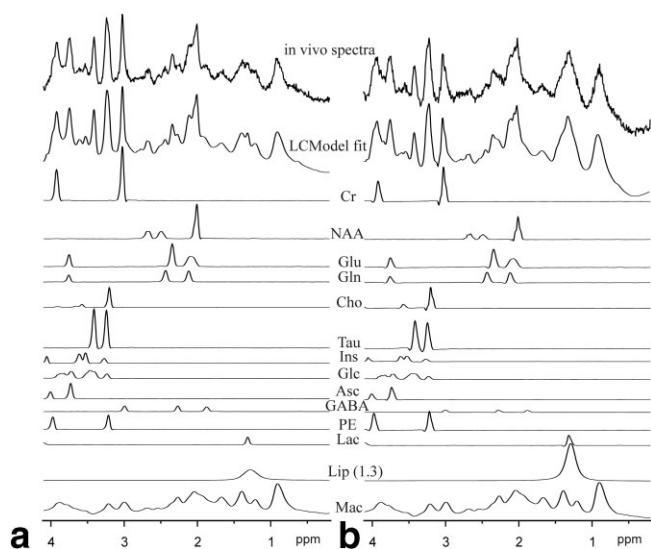
FIG. 5. LCModel fit of spectra from voxels located in penumbra (**a**) and in the edematous tissue (**b**) of a rat subjected to focal ischemia. The position of the voxels is depicted in Fig. 3. The individual fitted spectra of the most relevant metabolites, the lipid signal at 1.3 ppm, and the macromolecules are also shown.

Lac/Cr values calculated in the infarct region were uncertain because of a low SNR and increased linewidth.

DISCUSSION

As indicated previously (20), the SPECIAL selective excitation scheme providing increased SNR can be used not only for localized single-voxel spectroscopy but also for spectroscopic imaging. This study shows that a combination of a high-sensitivity quadrature surface coil and efficient shimming with the SPECIAL pulse sequence enables the acquisition of high-resolution quantitative maps of metabolites in rat brain. The spatial resolution of these maps is sufficient for measuring the neurochemical profile in subtle cerebral structures or for studying spatial distribution of changes in metabolite concentrations induced by a focal insult. The optimized experimental conditions allow a decrease in the volume necessary for determining the neurochemical profile at 1–2 μL spatial resolution with an echo time of a few ms. This volume size is comparable to that achieved in high-resolution positron emission tomography in rodents (27).

For achieving sufficient SNR in spectra measured from extremely small volumes, prolonged scan times are necessary. From this point of view the necessity to acquire the minimum number of two scans in each phase encoding step with the SPECIAL localization scheme is not restrictive. The measurement time can be further reduced by, e.g., elliptical sampling of the k-space.

The relatively short repetition time used in our protocol affects quantification of some metabolites. A brief calculation shows that if the true T_1 values of the metabolites lie in the range of 1.04–1.67 sec (25), this error is less than 6%. The error should be higher for Tau, which has a longer T_1 of 2.3 sec, and for Lip at 1.3 ppm having a shorter T_1 of about 0.6 sec. Thus, the concentrations of Tau and Lip shown in the metabolic maps in Fig. 3 should be multiplied by 1.25 and 0.85, respectively.

Compared to single voxel spectroscopy, which has achieved linewidths of 9–13 Hz over time in our laboratory at 9.4T (unpubl. obs.), the linewidth in spectra of some voxels was increased, due to uncompensated higher-order inhomogeneity terms. Instabilities, such as the drift of the static magnetic field, can increase the apparent linewidth due to the scan time on the order of 1 hr. Such instrumental limitations may have contributed to a less reliable quantification of pairs of metabolites having spectral lines with almost identical spectral appearance such as Cr/PCr or glycerophosphocholine/phosphocholine. Nevertheless, the data obtained on healthy rat brains demonstrate that shimming larger volumes with FASTMAP provides satisfactory linewidth over the entire volume with only small regions of increased inhomogeneity.

The high spatial resolution achieved with our protocol enables us to measure spectra from subtle and irregularly shaped cerebral structures such as the corpus callosum by summing spectra from voxels comprising the same tissue (28). An increase of SNR to 22–25 was observed in the spectra summed from six voxels. This increase was lower than the square root of the number of summed voxels,

Table 1
Absolute Concentrations of Brain Metabolites Averaged Over Three Rat Pups 36 hr After the Onset of Focal Ischemia

Metabolite	Concentration (mmol/kg)			
	Infarct region $n = 5^a$	Edematous tissue $n = 14$	Penumbra $n = 13$	Contralateral hemisphere $n = 13$
Cr	2.0 ± 1.2[b]	2.1 ± 1.6	7.3 ± 1.0	7.6 ± 0.5
NAA	1.3 ± 0.8	1.5 ± 1.1	5.3 ± 0.9	5.9 ± 0.4
Glu	2.9 ± 1.1	2.5 ± 1.8	6.6 ± 1.1	7.0 ± 0.7
Gln	1.4 ± 0.8	1.3 ± 1.0	3.7 ± 0.6	2.8 ± 0.3
Cho	1.0 ± 0.5	0.4 ± 0.2	1.1 ± 0.3	1.3 ± 0.2
Tau	1.5 ± 1.4	2.6 ± 1.8	8.6 ± 1.4	9.4 ± 1.2
Ins	—	0.6 ± 0.5	2.3 ± 0.5	3.5 ± 0.4
Glc	1.1 ± 0.7	1.7 ± 1.1	4.4 ± 0.6	4.7 ± 0.8
Lip (1.3 ppm)	34 ± 24	49 ± 25	22 ± 19	14 ± 9
Lac	1.0 ± 0.6	0.7 ± 0.5	1.0 ± 0.7	0.9 ± 0.3

[a]The number of voxels taken in statistics.
[b]Arithmetic mean ± standard deviation.

possibly due to correlation of instrumental components of the noise. The concentrations of Cr, Ins, Glx, and GABA in white matter (corpus callosum) were lower than those in gray matter (hippocampus), similar to observations in human brain (6,29,30).

Application of the technique to the rat brain with a local infarct demonstrates its high sensitivity in detecting changes of metabolite concentrations. When interpreting these metabolic maps one should be aware that the concentrations calculated for corner voxels of the depicted area are not reliable, as these voxels lay outside the active volume of the RF coil and had extremely low signal intensity. The overall high quality of spectra from individual voxels enabled us to quantify 10–13 metabolites with Cramer–Rao lower bounds less than 20%. The sharp boundary between higher and lower absolute metabolite concentrations in the metabolic maps coincides with the extent of edema in the anatomical images and illustrates the high spatial resolution. The decrease of the absolute metabolite concentrations in the edematous region was attributed to changes in concentrations rather than increased water content, which may result in overall underestimated metabolite concentrations, since the water signal was used as reference for quantification. However, water content can increase at most from 75% for white matter to 100% (cyst, CSF), which is several-fold smaller than the observed concentration changes. Moreover, the T_1 relaxation time of water in edema is typically longer than in normal brain tissue, which would reduce its signal due to T_1 saturation, offsetting the effect of increased water.

A highly resolved spatial distribution of the neurochemical profile in the infarct region and in the penumbra in rats with focal cerebral ischemia was observed and correlated with MR images and histology for the first time. Some of the observed changes in metabolite concentrations are in agreement with previous studies. The increase of lactate and lipids in the infarct region was found by Harada et al. (31) using localized proton spectroscopy. Similarly, a large increase in tissue choline concentration was reported in ischemic cortex (32). An increase of choline and free lipids in the ipsilateral striatum 2 weeks after 90-min middle cerebral artery occlusion in rats was also reported by Wang et al. (33). Using proton spectroscopic imaging, Igarashi et al. (34) reported a transient increase of Lac and Glu+NAA in both the ischemic core and rim, and of Gln+GABA in the ischemic rim 10 hr after the onset of permanent focal cerebral ischemia in rat. The increased Gln concentration was also observed by Haberg et al. (35) in an extract from ischemic rat penumbra. The larger extent of increased glutamine relative to increased glutamate likely reflects conversion of extracellular glutamate to glutamine by healthy astrocytes outside the ischemic region, consistent with increased excitotoxicity observed in hypoxic-ischemia. Changes in the activity of glutaminase and glutamine synthetase may also play a role (36). Confirmation of underlying mechanisms of such changes in distribution of these and other metabolites requires a more complete study that is beyond the scope of this article.

We conclude that measuring high-spatial-resolution quantitative metabolic maps is feasible on an animal scanner at ultra-short echo times, with the benefit that effects of transverse relaxation and J-evolution on the quantification can be neglected. The spatial resolution of the metabolic maps is comparable to that achieved on animal positron emission tomography scanners, e.g., for mapping the cerebral metabolic rate of glucose.

REFERENCES

1. Tkáč I, Starčuk Z, Choi IY, Gruetter R. In vivo ¹H NMR spectroscopy of rat brain at 1 ms echo time. Magn Reson Med 1999;41:649–656.
2. Pfeuffer J, Tkáč I, Provencher SW, Gruetter R. Toward an in vivo neurochemical profile: quantification of 18 metabolites in short-echo-time ¹H NMR spectra of the rat brain. J Magn Reson 1999;141:104–120.
3. Geppert C, Dreher W, Leibfritz D. PRESS-based proton single-voxel spectroscopy and spectroscopic imaging with very short echo times using asymmetric RF pulses. Magn Reson Mater Phy 2003;16:144–148.
4. Seeger U, Klose U, Seitz D, Nagele T, Lutz O, Grodd W. Proton spectroscopy of human brain with very short echo time using high gradient amplitudes. Magn Reson Imaging 1998;16:55–62.
5. Lentz MR, Taylor JL, Feldman DA, Cheng LL. Current clinical applications of in vivo magnetic resonance spectroscopy and spectroscopic imaging. Curr Med Imag Rev 2005;1:271–301.
6. McLean MA, Woermann FG, Barker GJ, Duncan JS. Quantitative analysis of short echo time ¹H-MRSI of cerebral gray and white matter. Magn Reson Med 2000;44:401–411.
7. Xu D, Chen AP, Cunningham C, Osorio JA, Nelson SJ, Vigneron DB. Spectroscopic imaging of the brain with phased-array coils at 3.0 T. Magn Reson Imaging 2006;24:69–74.
8. Otazo R, Mueller B, Ugurbil K, Wald L, Posse S. Signal-to-noise ratio and spectral linewidth improvements between 1.5 and 7 Tesla in proton echo-planar spectroscopic imaging. Magn Reson Med 2006;56:1200–1210.
9. McNab JA, Bartha R. Quantitative short echo-time ¹H LASER-CSI in human brain at 4 T. NMR Biomed 2006;19:999–1009.
10. McLean MA, Woermann FG, Simister RJ, Barker GJ, Duncan JS. In vivo short echo time ¹H-magnetic resonance spectroscopic imaging (MRSI) of the temporal lobes. Neuroimage 2001;14:501–509.
11. Woermann FG, McLean MA, Bartlett PA, Barker GJ, Duncan JS. Quantitative short echo time proton magnetic resonance spectroscopic imaging study of malformations of cortical development causing epilepsy. Brain 2001;124:427–436.
12. Simister RJ, Woermann FG, McLean MA, Bartlett PA, Barker GJ, Duncan JS. A short-echo-time proton magnetic resonance spectroscopic imaging study of temporal lobe epilepsy. Epilepsia 2002;43:1021–1031.
13. Rijpkema M, Schuuring J, van der Meulen Y, van der Graaf M, Bernsen H, Boerman R, van der Kogel A, Heerschap A. Characterization of oligodendrogliomas using short echo time ¹H MR spectroscopic imaging. NMR Biomed 2003;16:12–18.
14. Kim DH, Barkovich AJ, Vigneron DB. Short echo time MR spectroscopic imaging for neonatal pediatric imaging. Am J Neuroradiol 2006;27:1370–1372.
15. Soher BJ, Vermathen P, Schuff N, Wiedermann D, Meyerhoff DJ, Weiner MW, Maudsley AA. Short TE in vivo ¹H MR spectroscopic imaging at 1.5 T: acquisition and automated spectral analysis. Magn Reson Imaging 2000;18:1159–1165.
16. Juchem C, Logothetis NK, Pfeuffer J. High-resolution ¹H chemical shift imaging in the monkey visual cortex. Magn Reson Med 2005;54:1541–1546.
17. Liimatainen T, Hakumaki J, Tkáč I, Grohn O. Ultra-short echo time spectroscopic imaging in rats: implications for monitoring lipids in glioma gene therapy. NMR Biomed 2006;19:554–559.
18. von Kienlin M, Ziegler A, Le Fur Y, Rubin C, Decorps M, Remy C. 2D-spatial/2D-spectral spectroscopic imaging of intracerebral gliomas in rat brain. Magn Reson Med 2000;43:211–219.
19. Ziegler A, von Kienlin M, Decorps M, Remy C. High glycolytic activity in rat glioma demonstrated in vivo by correlation peak ¹H magnetic resonance imaging. Cancer Res 2001;61:5595–5600.
20. Mlynárik V, Gambarota G, Frenkel H, Gruetter R. Localized short-echo-time proton MR spectroscopy with full signal-intensity acquisition. Magn Reson Med 2006;56:965–970.
21. Renolleau S, Aggoun-Zouaoui D, Ben-Ari Y, Charriaut-Marlangue C. A model of transient unilateral focal ischemia with reperfusion in the P7 neonatal rat: morphological changes indicative of apoptosis. Stroke 1998;29:1454–1460.

22. Gruetter R, Tkáč I. Field mapping without reference scan using asymmetric echo-planar techniques. Magn Reson Med 2000;43:319–323.

23. Pohmann R, von Kienlin M. Accurate phosphorus metabolite images of the human heart by 3D acquisition-weighted CSI. Magn Reson Med 2001;45:817–826.

24. Provencher SW. Estimation of metabolite concentrations from localized in vivo proton NMR spectra. Magn Reson Med 1993;30:672–679.

25. de Graaf RA, Brown PB, McIntyre S, Nixon TW, Behar KL, Rothman DL. High magnetic field water and metabolite proton T_1 and T_2 relaxation in rat brain in vivo. Magn Reson Med 2006;56:386–394.

26. Bruhn H, Frahm J, Gyngell ML, Merboldt KD, Hanicke W, Sauter R. Cerebral metabolism in man after acute stroke: new observations using localized proton NMR spectroscopy. Magn Reson Med 1989;9:126–131.

27. Park SJ, Rogers WL, Huh S, Kagan H, Honscheid K, Burdette D, Chesi E, Lacasta C, Llosa G, Mikuz M, Studen A, Weilhammer P, Clinthorne NH. Performance evaluation of a very high resolution small animal PET imager using silicon scatter detectors. Phys Med Biol 2007;52:2807–2826.

28. Gruber S, Stadlbauer A, Mlynárik V, Gatterbauer B, Roessler K, Moser E. Proton magnetic resonance spectroscopic imaging in brain tumor diagnosis. Neurosurg Clin N Am 2005;16:101–114.

29. Jensen JE, Frederick BD, Renshaw PF. Grey and white matter GABA level differences in the human brain using two-dimensional, J-resolved spectroscopic imaging. NMR Biomed 2005;18:570–576.

30. McLean MA, Barker GJ. Concentrations and magnetization transfer ratios of metabolites in gray and white matter. Magn Reson Med 2006; 56:1365–1370.

31. Harada K, Honmou O, Liu H, Bando M, Houkin K, Kocsis JD. Magnetic resonance lactate and lipid signals in rat brain after middle cerebral artery occlusion model. Brain Res 2007;1134:206–213.

32. Scremin OU, Jenden DJ. Focal ischemia enhances choline output and decreases acetylcholine output from rat cerebral cortex. Stroke 1989; 20:92–95.

33. Wang X, Qian J, He R, Wei L, Liu N, Zhang Z, Huang Y, Lei H. Delayed changes in T_1-weighted signal intensity in a rat model of 15-minute transient focal ischemia studied by magnetic resonance imaging/spectroscopy and synchrotron radiation X-ray fluorescence. Magn Reson Med 2006;56:474–480.

34. Igarashi H, Kwee IL, Nakada T, Katayama Y, Terashi A. [1]H magnetic resonance spectroscopic imaging of permanent focal cerebral ischemia in rat: longitudinal metabolic changes in ischemic core and rim. Brain Res 2001;907:208–221.

35. Haberg A, Qu H, Saether O, Unsgard G, Haraldseth O, Sonnewald U. Differences in neurotransmitter synthesis and intermediary metabolism between glutamatergic and GABAergic neurons during 4 hours of middle cerebral artery occlusion in the rat: the role of astrocytes in neuronal survival. J Cereb Blood Flow Metab 2001;21: 1451–1463.

36. Ramonet D, Rodriguez MJ, Fredriksson K, Bernal F, Mahy N. In vivo neuroprotective adaptation of the glutamate/glutamine cycle to neuronal death. Hippocampus 2004;14:586–594.